Novel Mixing Tank for Improved Gas–Liquid Mass Transfer and Solids Suspension

Harvey J. Palmer, Christine M. C. Hughes, Martin Lessen, Jennifer Greenleaf, Kristen L. Buehler, and Carmen Villalobos
Dept. of Chemical Engineering, University of Rochester, Rochester, NY 14627

A novel, baffleless, mixing tank configuration presented provides greater mixing efficiency than conventional technologies under a wide variety of operating conditions. The concept uses a cylindrical tank with a contoured bottom and a shroud that surrounds an axial flow impeller and supports a set of stationary "antiswirl" fins positioned in close proximity to the impeller blades. The angle and pitch of the fins impart an angular component to the flow that is equal and opposite to the swirl induced by impeller rotation, thereby eliminating the need for wall baffles. The contoured bottom eliminates dead spaces beneath the impeller and in the corners of flat-bottom mixing tanks. This alternative mixing system, named the ASSET system, is compared to conventional mixing configurations through experiments of power consumption, gas–liquid mass transfer, and solids suspension. Measurements of Power number vs. Reynolds number reveal that it has power requirements similar to those of high-efficiency axial-flow turbines in a conventional tank geometry. Unsteady-state oxygen absorption and stripping experiments are used to determine the interphase mass-transfer coefficient as a function of power input for each configuration at superficial gas feed velocities of 0.057 to 0.17 cm/s. With this system, $K_L a$ values are on average 30 to 50% greater than those obtained in a conventional mixing tank at the same power input. Measurements of the height of the well-mixed region of suspended solids in a 15 wt. % mixture of 0.1-cm-dia. glass beads in water indicate that the ASSET system requires ~ 30% less power to achieve equivalent extents of solids suspension than the conventional setup.

Introduction

Mixing is an integral part of chemical processes. The manufacturing methods for most products require the blending of raw materials. Often the substances to be mixed are in separate phases, necessitating that gases, liquids, and solids be mixed together in an efficient, effective manner that promotes interphase heat and mass transfer. Thus, any innovation in mixing technology that can provide equivalent mixing effectiveness with less energy consumption is certain to be of significant value to the chemical-process industry. The demand for improved mixing systems is driven only partly by the desire to minimize energy consumption. The materials and conditions used in a particular process may require special mixing considerations. For example, in the biotechnology industry there is a need to devise methods to provide high rates of oxygen transfer in gas–liquid–cell dispersions at low agitation rates so that the fragile cells being cultivated are not damaged by the intensity of turbulence in the mixing process.

Generally, the mixing of materials in both single and multiphase systems is done in a cylindrical, flat-bottom tank with wall baffles and an impeller that is rotated on a shaft at the center line of the tank (cf. Nagata, 1975; Oldshue, 1983). This classic mixing-tank configuration can be traced back to preindustrial times, and it has been the standard in the chemical industry for nearly a century. Nevertheless, there are features inherent to this system that limit its effectiveness. These include areas of stagnation beneath the impeller, behind the wall baffles, and in the corners of the tank, and an angular (rotational) component in the flow pattern that inhibits mixing. The research literature on mixing is replete with examples of improved designs for the agitator or impeller, the shape of the tank, the location and size of wall baffles, the

Correspondence concerning this article should be addressed to H. J. Palmer.
Present addresses of: Christine Carpenter Hughes, DuPont Specialty Chemicals, DuPont Chambers Works, Deepwater, NJ 08023; M. Lessen, Yates Memorial Professor of Engineering, Emeritus, 12 Country Club Drive, Rochester, NY 14618.

introduction of draft tubes to promote the recirculation of fluid in the tank, and various methods and locations for gas introduction with respect to the impeller (Bakker and VandenAkker, 1990; Hyman, 1962; Jahoda and Machon, 1994; Jameson, 1962; Mann, 1985; Oldshue, 1965; Oldshue et al., 1988; Yoshida, et al., 1996; Zhou and Kresta, 1996). In particular, such research has led to the development of axial flow impellers with a discharge velocity profile that is truly aligned with the axis of rotation and, if desired, a flow rate that is essentially independent of radial position below the impeller. Regarding the shape of the tank, attention has focused on the advantages of a contoured tank bottom, with the intention of eliminating the stagnation zones in the tank corners where material can accumulate and deteriorate. For example, Aeschbach and Bourne (1972) investigated the benefits of alternative tank shapes and agitator/baffle configurations on the particle-size distribution produced in a crystallizer. Their results demonstrated that a more uniform particle-size distribution is obtained with a mixing configuration that employs a concave tank bottom, traditional wall baffles, a draft tube to assure full turnover in the tank, and an axial flow impeller oriented to pump the suspension upward.

Despite the myriad experiments presented in the literature, however, to our knowledge no one other than Aeschbach and Bourne has attempted to *integrate* improved designs of the impeller, the tank shape, and the baffles to produce optimized configurations for specific mixing applications. In this article, we present our first attempts at creating just such an integrated design. The key elements of our new mixing configuration and the rationale for the design are presented below, followed by experimental results that clearly show the efficacy of the design through power consumption and gas–liquid mass-transfer experiments.

New Mixing-Tank Configuration

The patented mixing configuration investigated in this study is shown in Figure 1 (see also Lessen, 1995): we call it the *ASSET* system for its *a*nti*s*wirl *s*tator and *e*ngineered *t*ank. It consists of a 61.0-cm (24-in.) diam, cylindrical Plexiglas tank fitted with a contoured bottom and a shroud assembly that surrounds an axial-flow impeller, which is rotated (clockwise) in the usual manner to produce a downward flow. The shroud assembly is composed of six stationary antiswirl fins that are attached to a thin-walled, cylindrical, stainless-steel shell. The shell surrounds, supports, and helps to maintain the shape of the fins in their position just above the impeller blades. The diameter of the shell (20.4 cm) is slightly larger than the impeller (19.3 cm in diameter), and its height is just sufficient to enclose both the impeller and the fins (7.6 cm for the A310 impeller and 12.7 cm for the A410 impeller). To fix the position of the shroud, with the antiswirl fins just above the impeller, the inside edge of each fin is attached circumferentially to the bottom of a section of 7.5-cm OD PVC pipe (2.5 in. nominal). The other end of the pipe, in turn, is attached to brackets so that the entire unit (composed of the pipe, fins, and shroud) can be suspended from the top edge of the tank, with the pipe positioned vertically along the center line of the tank, surrounding the impeller shaft. Photographs of the shroud assembly, showing the fins and their attachment to the shell and central pipe, are presented in Figure 2.

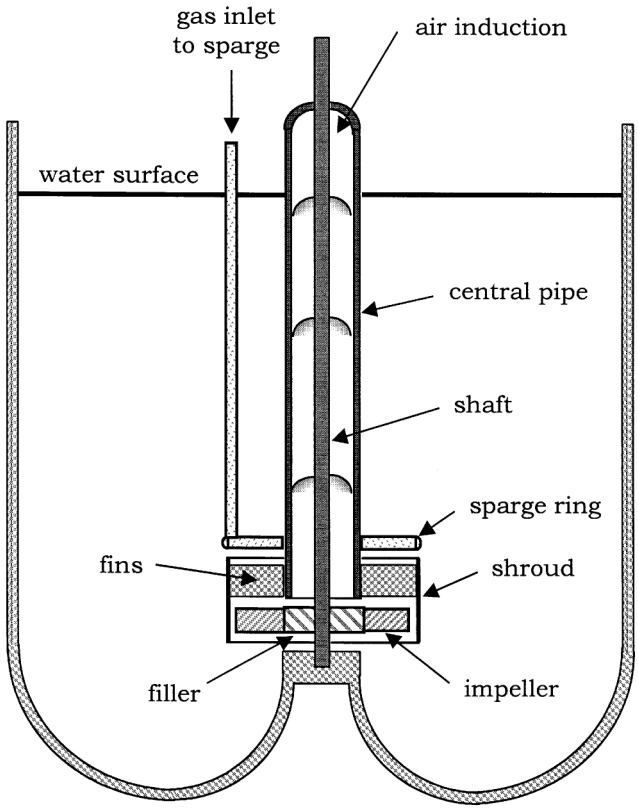

Figure 1. *ASSET* system.

The six fins are fabricated of 25-μm-thick, malleable stainless-steel sheet metal, and are cut in a trapezoid-like shape $\sim$ 6.5 cm long, with sides that are $\sim$ 3.9 cm and $\sim$ 5.9 cm in length, with tabs protruding from the sides of the "trapezoid" (see Carpenter, 1998, for the precise shape). These tabs are bent at a right angle to the fin for attachment to the shell and the PVC pipe, the attachment being made with small machine screws and nuts, with the shorter side of the fin attached to the shell. Prior to bending the tabs, each fin is put through a roller/shape device to add a radius of curvature of $\sim$ 4.5 cm in the plane perpendicular to the top edge of the fin. The fins are then mounted between the shell and the PVC pipe such that the tangent plane to the fin at its *bottom* edge makes a 60° angle with the horizontal where the fin attaches to the shell, and a 45° angle where it attaches to the PVC pipe. The radius of curvature of the fin is appropriate if the tangent plane to the fin at its *top* edge is vertical. The angle and pitch of the antiswirl fins are chosen to introduce an angular component to the flow in the vicinity of the impeller that is equal and opposite to the angular motion induced by the impeller rotation. Hence, the stator blades and the impeller rotation combine to produce a discharge liquid flow that has almost no rotational velocity, thereby eliminating the need for baffles on the tank walls. (The specific geometric details of fin size and shape presented here were refined by trial and error.) The use of the antiswirl fins in place of wall baffles is an appealing feature because, unlike traditional baffles, the fins interact directly with *all* the liquid that is pumped by the impeller. Furthermore, the close proximity of the fins to the impeller creates a more substantial region

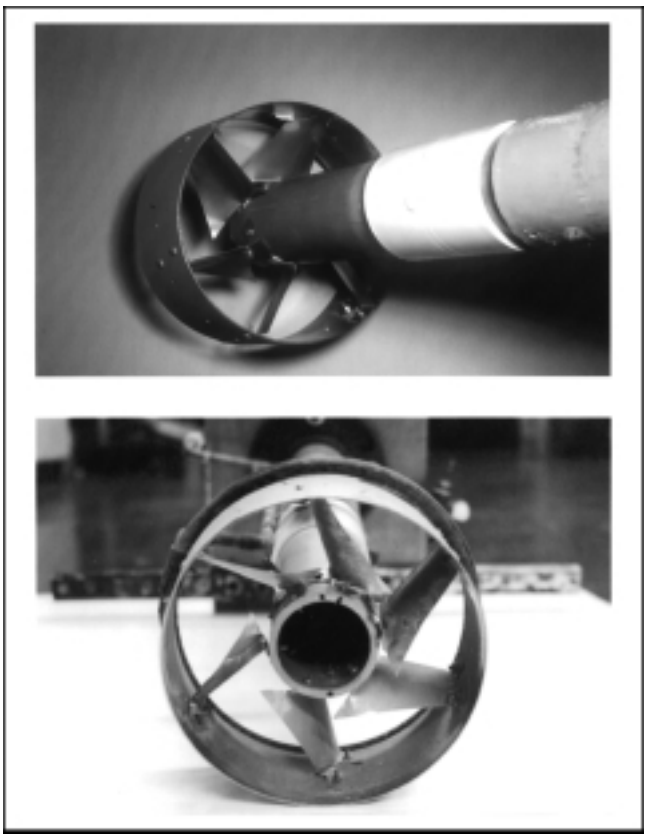

Figure 2. Two views of the shroud unit for the *ASSET* system.

It shows the contoured shape of the fins and their attachment to both the shroud and central pipe: looking into shroud assembly (a) from above, and (b) from below.

of high shear in the tank that, in the case of gas–liquid dispersions, appears to be especially effective for inducing bubble (or drop) breakup, thereby promoting interphase mass transfer.

The hemitoroidal, concave tank bottom extends between a vertical, cylindrical inner neck (or hub), that is 7.5 cm in diameter and 15.2 cm high, and the wall of the cylindrical tank. Ideally, the hemitoroidal profile of the tank bottom would have a monotonically increasing toroidal radius of curvature between the neck and the tank wall. For simplicity of fabrication, however, the tank bottom tested is composed of two circular arcs: an inner radius of 11.4 cm and an outer radius of 15.2 cm (equal to one-half the radius of the tank). With these two radii of curvature, there is no discontinuity in the slope of the bottom surface of the tank. In addition, the bottom surface is tangent to both the neck and the tank wall on the circumferences where the bottom meets these vertical boundaries. The objective is to have the shape match to the greatest extent possible the circulation pattern created by the impeller, so that "dead zones" of fluid recirculation are eliminated. In this sense, the new design builds upon the favorable results of Aeschbach and Bourne (1972) in their crystallization experiments. In addition, the curvature of the tank bottom favors the formation of Görtler vortices and other fluid instabilities in the momentum boundary layer along its concave surfaces (Görtler, 1941; see also Schlichting, 1968). These instabilities disrupt the boundary layer along the tank bottom, to provide a scrubbing action that increases the rate of heat transfer through the bottom, inhibits fouling, and maintains solids suspension at very low fluid velocities and minimal power input.

As shown in Figure 1, the central pipe that supports the shroud assembly is aligned with the hub in the contoured bottom and extends upward through the liquid surface. Because the rotation of the impeller creates a region of low pressure on the inlet side of the impeller, there is a pressure difference across the length of this central pipe. At sufficiently high impeller speeds, this pressure difference is sufficient to overcome the hydrostatic pressure in the tank and draw atmospheric air down the pipe. This feature is advantageous in moderate-size vessels if aeration is desired, and thus the benefits of this phenomenon were assessed in our mass-transfer experiments. However, in order to measure the performance of the *ASSET* system at specific gas feed rates, for direct comparison to conventional geometries, the *ASSET* system was normally operated with a shaft seal installed at the top of the central pipe. This shaft seal was made of 6-mm-thick silicone gasketing material with a central hole cut in it with a cork borer of a size just slightly smaller than the diameter of the impeller shaft. A high-temperature silicone lubricant was used to minimize the frictional drag of the gasket on the shaft. The magnitude of the drag produced by the shaft seal was determined by measuring the power input vs. impeller speed with and without the shaft seal under otherwise identical circumstances.

The impeller and shroud are positioned such that the bottom of the impeller was $\sim$18 cm above the bottom of the tank. A sleeve bearing is added to the top of the cylindrical hub to support the end of the impeller shaft for increased stability. Liquid depth in the tank is 61.3 cm, equal to the tank diameter, resulting in a total liquid volume of $\sim$0.16 m^3. Gas is supplied to the tank, when desired, through a ring-shaped sparger positioned directly above the shroud. The sparge ring has an ID of 11.4 cm and is fabricated of 1.3-cm-OD soft copper tubing with 58 outlet holes 0.15 cm in diameter.

Two axial-flow impellers were used with the *ASSET* system in our experiments: the *Lightnin* A310 and A410 impellers, both 19.3 cm in diameter (see Figure 3). Both impellers produce a uniform axial-discharge-velocity profile with three cambered and twisted blades, part parallel and part twisted. However, the surface area of the blades of the A410 impeller are $\sim$2.5 times that of the A310 impeller (that is, it has a higher solidity), making the A410 much more effective at dispersing gas in the tank at high gas feed rates. Since the center of the tank is occupied by the 7.5-cm-diameter pipe and hub, impeller blade area in this region is superfluous. Thus, the center of the A310 impeller was filled with a disk of fiberglass 7.5 cm in diameter to minimize energy dissipation, thereby reducing the effective length of the impeller blades to 6 cm on this modified A310 (see Figure 3). Because the A410 impeller came with an enlarged hub section, the A410 was not modified.

The conventional tank configuration used for the baseline experiments consisted of a standard flat-bottom cylindrical tank 60 cm in diameter, equipped with four, evenly spaced wall baffles 5 cm in width. The tank was filled to a depth of

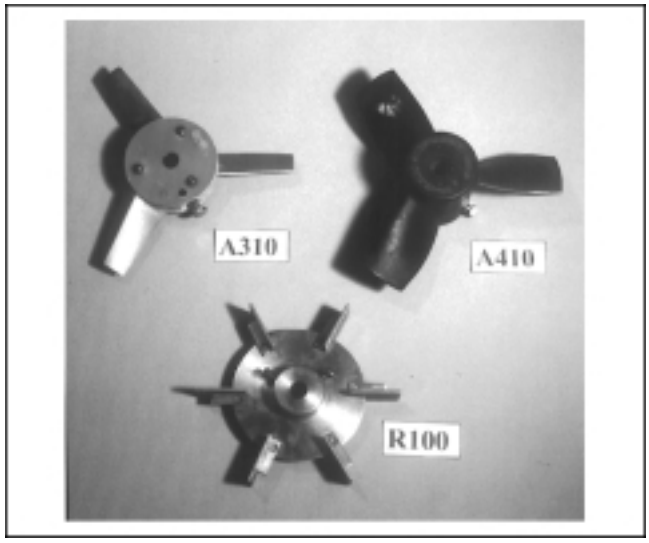

Figure 3. Impellers used during the course of this research:

(a) Low solidity, axial flow Lightnin A310; (b) high solidity, axial flow Lightnin A410; (c) flat blade, disk-type radial flow Lightnin R100. Notice the central disk on the A310 that was added to match the diameter of the central pipe of the *ASSET* system.

60 cm with ~ 0.17 m^3 of water. In addition to the A310 and A410 impellers, experiments were done utilizing a 15.2-cm-diameter *Lightnin* R100 radial-flow impeller. The R100 impeller, or Rushton turbine, has six blades and is shaped like a paddle wheel. It is used in this study because it is used extensively in the industry for dispersing gas in liquids. In all experiments, the impeller was placed a distance equal to one impeller diameter off the tank bottom. A sparge ring identical to the one described earlier was placed just below the impeller for gas addition.

Experimental Apparatus

All experiments were done with the aid of a *Lightnin* Laboratory Dynamometer Workstation that consists of a variable-speed, hollow-shaft motor mounted on a bearing platform, a dynamometer spring scale to measure the torque delivered to the impeller shaft by the motor, and an adjustable-platform lift table to support the tank. The spring scale has a limit of 10 lb_f and a lever arm of 0.0794 m, that together place an upper limit of 3.532 J on the torque measurement. The cylindrical tank was centered on the lift table and filled with water, previously purified by reverse osmosis, to a height equal to the tank diameter. The impeller, shaft, sparge ring, and shroud assembly (if applicable) were placed in the tank and centered appropriately. The speed of the impeller shaft was measured with a photo-sensor, interfaced to a microcomputer, that detects the frequency of passage of a mark on the motor shaft, with readings of impeller speed recorded every 1.5 s. The effectiveness of each mixing system to promote interphase mass transfer was evaluated with unsteady-state oxygen uptake and stripping experiments. In these experiments, the instantaneous oxygen concentration in the liquid was monitored with a YSI Model 57 oxygen probe located ~ 7 cm from the tank wall and midway between the tank bottom and the water surface. The probe was oriented face down (with the face at a slight angle to the horizontal) so that the upward flow of liquid near the cylindrical wall would impinge on the face of the probe and sweep gas bubbles from the surface of the sensor membrane. This probe was also interfaced to the microcomputer, with readings recorded every 1.5 s.

The rate of gas flow to the sparge ring in the tank was measured with a calibrated rotameter. Two manually operated valves were located upstream of the rotameter. The first was used to select the type of gas to be added to the tank (air or nitrogen) and the second was used to control the gas flow rate to the sparge ring. The air that was used in all of the oxygen uptake and flooding experiments was obtained from a university-operated compressed-air system (water pumped and filtered) for the building. The nitrogen that was used in the stripping experiments was obtained commercially in compressed-gas cylinders. For both gases, regulators were used to control the pressure of the gas flowing to the tank.

Methods and Results

Power-consumption measurements

Power-consumption data were obtained for both the *ASSET* system and the conventional tank configuration at various gas rates and impeller speeds. Power data were also collected during every gas–liquid mass-transfer experiment. To determine the power as a function of impeller speed, the torque required to keep the drive motor stationary is measured with the dynamometer spring scale, and the power computed as the product of torque and the rotational speed of the impeller. The measurements of power as a function of impeller speed are then plotted in terms of the Power number vs. the Reynolds number:

$$\text{Reynolds number} = \frac{104.7\omega D^2\gamma}{\mu}$$

$$\text{Power number} = \frac{0.8708(P)}{\omega^3 D^5 \gamma},$$

where the impeller diameter D is in meters, its rotational speed ω is in rev/min (rpm), the power P is in W, the liquid's specific gravity γ is dimensionless, and its viscosity μ is in Pa·s. Both Power number and Reynolds number are dimensionless (cf. Nagata (1975), for theoretical models, correlations, and additional methods of measuring power consumption).

The experimental measurements of Power number vs. Reynolds number for the various mixing-tank configurations examined in this study are shown in Figure 4. The first thing that is evident from this figure is that the Power number is essentially independent of the Reynolds number for each configuration. This functionality is characteristic of the turbulent flow regime in a mixing tank. A second observation is that the radial-flow R100 impeller draws significantly more power than any of the axial-flow impeller systems at a given impeller speed (fixed Reynolds number). This well-recognized feature of radial-flow impellers occurs primarily because the liquid discharges from the impeller at right angles

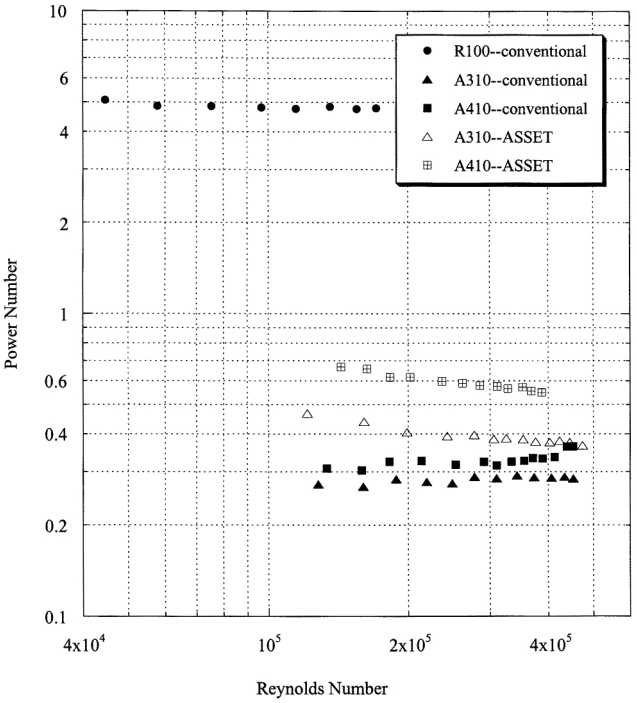

Figure 4. Power number vs. Reynolds number curves for various impellers in the conventional tank configuration and *ASSET* system.

from its inlet path to the impeller region, thereby dissipating all of its linear momentum. By contrast, the inlet and outlet flows from an axial-flow impeller are in the same direction. Looking now at the relative performance of the two axial-flow impellers in the conventional tank configuration, we see that the A410 impeller draws slightly more power than the A310 impeller at the same impeller speed because of its higher solidity (cf. Rushton et al., 1950a,b, for a discussion of the influence of impeller design on power consumption).

Now let us focus on the distinction between the *ASSET* system and the conventional configuration equipped with an axial-flow impeller. In this regard, it is evident from Figure 4 that at a given impeller speed the *ASSET* system draws significantly more power than the conventional tank configuration when the two are equipped with the same axial-flow impeller. In particular, the Power number for the *ASSET* system is 0.38 with the A310 impeller and ~ 0.54 with the A410 impeller, as compared to values of 0.28 and 0.32, respectively, for its conventional counterpart. This result was not expected, because the antiswirl stator blades have significantly less surface area than the wall baffles in the conventional setup, thereby leading one to anticipate less, rather than greater, energy dissipation. On the other hand, the antiswirl stators deflect rapidly moving fluid, whereas the conventional baffles act on slow-moving fluid near the tank walls. Another argument in favor of the higher rate of energy consumption in the *ASSET* system is as follows: all the liquid being pumped by the axial-flow impeller in the *ASSET* system must first pass through the stator blades, which impart an angular (counterclockwise) velocity component to the flow. Thus, the liquid entering the impeller has a nonaxial component of momentum that must be removed by the impeller.

As stated earlier, the rotation of the impeller in the *ASSET* system creates a region of low pressure at the bottom of the central pipe, causing air to be sucked down the pipe and into the liquid in the tank. This phenomenon is particularly noticeable with the higher solidity, A410 impeller, and the large amount of air that is drawn down the central tube at high impeller speeds reduces the power consumption of the impeller by a significant amount. Visual observations indicate that the *ASSET* system with the A410 impeller begins to draw in air at an impeller speed of ~ 550 rpm. At 700 rpm, the volume of air drawn into the tank is sufficient to reduce the amount of power required by almost 17%. When we need to prevent this air induction from occurring, a shaft seal is installed at the top of the central pipe. This seal is lubricated with high vacuum silicone grease; nevertheless, the friction caused by the seal on the shaft is sufficient to increase the torque readings at low power inputs, namely at Reynolds less than $\sim 200{,}000$. By measuring torque vs. rpm in an empty tank with the shaft seal in place, the effect of this frictional force (which is ~ 0.9 N), is easily accounted for. Alternately, for Reynolds numbers $< 300{,}000$, the shaft seal is unnecessary, and thus the power input required for mixing can be measured as a function of gas feed rate without any uncertainty about the net rate of gas flow into the tank. On the other hand, for Reynolds numbers $> 300{,}000$, the shaft seal is needed to prevent excess air from entering the tank, but the frictional force due to the shaft seal is insignificant relative to the torque required to turn the impeller in the water.

Gas handling and flooding

In conventional tank configurations, it is well known that low-solidity axial-flow turbines are prone to flooding when gas is sparged into the tank. At all impeller speeds, a region of low pressure exists behind each impeller blade where pockets of air become trapped. If the rate of gas addition to the tank is sufficiently high at a given impeller speed, the amount of air trapped in the impeller region will become so large as to engulf all the impeller blades and thereby block the flow of liquid through the impeller. The net result is a drastic reduction in the pumping rate of the impeller and the liquid circulation rate in the tank. Because the presence of the shroud assembly around the impeller is expected to exacerbate this effect, one goal in our study was to compare the ability of the *ASSET* system to handle high gas input rates with that of conventional configurations. In this assessment, flooding points were determined by varying the power input and thus the impeller speed, at a constant gas flow rate. The flooding point was defined as the highest power at which the impeller became flooded in less than two minutes at a particular gas flow rate. A sharp drop in torque and a rise in impeller rpm indicated when the impeller was flooded. The flooding point could also be observed visually as a severe decrease in the ability of the impeller to redistribute gas throughout the tank, a significant decrease in the extent of liquid recirculation patterns, and a "whooshing" sound as the impeller began to flood.

Flooding points were found for gas feed rates of 10–40 L/min (that is, superficial gas velocities of from 0.057 cm to 0.23 cm/s) using either the modified A310 or the A410 impeller in the *ASSET* system and an unmodified A310 im-

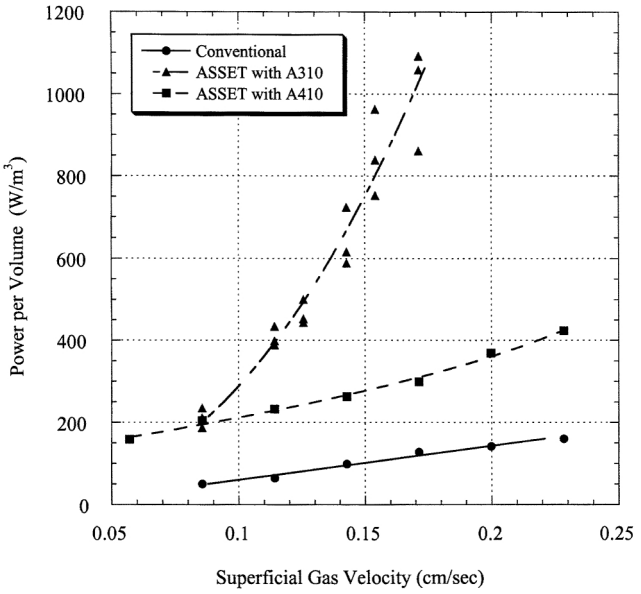

Figure 5. Flooding data for the ASSET system equipped with the modified A310 or A410 impeller, with equivalent data for the conventional configuration with an A310 impeller.

At a given gas flow rate, the data represent the highest power at which the impeller still floods within 2 min. Thus, the region above each curve represents operating conditions for which the impeller does not flood for the applicable mixing setup.

peller in the conventional configuration. These results are presented in Figure 5. Notice that the presence of the shroud assembly accentuates the general tendency of the A310 impeller to flood with gas. However, a major improvement in gas handling ability with the *ASSET* system is achieved by using an A410 impeller. Nevertheless, the *ASSET* system has greater difficulty than a conventional tank configuration in dispersing gas at large gas feed rates to the tank because the presence of the antiswirl fins and the cylindrical shell increase the probability that air will become trapped in the shroud area. This greater tendency toward flooding also may be due in part to the fact that gas bubbles in the *ASSET* system cycle through the impeller more than once, increasing the gas holdup in the tank and the gas load on the impeller.

Gas–liquid mass-transfer rates

The relative ability of the various mixing configurations to promote interphase mass transfer in gas–liquid dispersions was determined by doing unsteady-state oxygen absorption and desorption experiments, and then computing the overall mass-transfer coefficient, K_La (cf., Linek, et al., 1987; and Lee and Foster, 1990, for overviews of the methods for determining and characterizing the rate of oxygen transfer in mechanically agitated tanks). In an oxygen-absorption (uptake) experiment, the liquid in the tank is first stripped of all dissolved oxygen by bubbling nitrogen into the tank through the sparge ring at 20 to 30 L/min for at least 15 min while stirring at 550–650 rpm. The gas flow rate and impeller speed are then adjusted to their desired values for the experiment. When the system reaches equilibrium, as indicated by a constant, near-zero oxygen sensor reading, the data-acquisition program on the microcomputer is initiated, allowing the impeller speed and dissolved-oxygen concentration (DOC) to be recorded. After ~ 60 s, the source of gas is quickly switched from nitrogen to air and the gas flow rate is rapidly, but carefully, adjusted to the desired level. Each experiment is run until the DOC reaches a constant value (which is approached asymptotically) and remains at this saturation value C^* for several minutes. Overall, at least 15 min elapse from the time that the data-acquisition system is initiated to the time that sufficient data have been collected to substantiate the final C^* value. Then an analogous desorption (stripping) experiment is initiated by quickly switching the source of the gas back to pure nitrogen and recording the decrease in DOC with time until a stable, final value of DOC is achieved (very close to zero).

The DOC data, recorded at 1.5-s intervals during each experiment, are used to determine the overall volumetric mass-transfer coefficient for interphase transfer, K_La, as defined by the following equation:

$$\frac{d}{dt}(C) = K_La(C^* - C),$$

where C denotes the dissolved oxygen concentration in the liquid phase at any instant, and C^* is the dissolved oxygen concentration in equilibrium with the gas being fed to the tank. Integration of the preceding equation yields the following result, which describes the DOC as a function of time:

$$\ln \frac{(C^* - C)}{(C^* - C_0)} = -K_La(t), \tag{1}$$

where C_0 is the value of the DOC at the start of the experiment. Since C^*, C, and C_0 are all measured in the experiment, the K_La can be determined by plotting $-\ln[(C^* - C)/(C^* - C_0)]$ vs. time for the transient experiment. The slope of the resulting line is the K_La at the experimental conditions. The values for C_0 and C^* are determined by averaging the raw data obtained for the first and last 60 s of the experiment, respectively. The semilog plot of the data, as per Eq. 1, yields a very straight line over the entire transient-response range (cf. Carpenter, 1998, for more details). But the data become scattered as the equilibrium condition is approached, owing to the fact that the experimental error in detecting DOC is of the same order as the difference between C and C^*. Thus, in our least-squares regression algorithm, we use the data for $(C^* - C)/(C^* - C_0)$ between 0.95 and 0.10. Any error associated with the finite response time of the DO probe was negligible in comparison to the scatter in the mass-transfer results. We measured the rate constant of the probe to be 0.2 s^{-1}, which is an order of magnitude faster than all but our highest measured values of K_La (that is, those obtained with the *ASSET* system at 30 L/min). Even at these conditions, we obtained a straight line (with no hint of curvature) in our semilog plot.

Because the rate of mass transfer is temperature sensitive, the water temperature was measured during each experiment. Although the temperature during any particular experiment was essentially constant, the operating temperature did

vary from 20°C to 28°C, because precise temperature control from one day to the next was impractical. Instead, to provide a direct comparison of the measured K_La values on an equivalent basis, all K_La values were corrected to 20°C with the well-accepted correction

$$(K_La)_{20^\circ} = \frac{(K_La)_T}{(1.024)^{T-20^\circ}},$$

where T is the temperature in degrees Celsius (Eckenfelder, 1966). Several oxygen uptake and stripping experiments were done over a temperature range of 16° to 44°C to examine the validity of this correlation, and the measured K_La values vs. temperature were in very good agreement with this equation (cf., Carpenter, 1998, for more details).

As stated earlier, both absorption and desorption (stripping) experiments were done sequentially at a common set of mixing conditions. Because the rate of oxygen transport should depend upon the turbulent intensity in the tank, the gas holdup, the bubble-size distribution, *but not on the direction of mass transport*, the value of K_La obtained from the stripping experiment should compare favorably with that from the uptake (absorption) experiment. Countless experiments in our lab over the past several years validate this hypothesis. The most significant source of error in the determination of K_La is the uncertainty in the measured values of C^* and C_0. To obtain an estimate of the percent error caused by this uncertainty, the values of C^* and C_0 for each experiment were averaged, respectively, for all runs performed on a single day, and the standard deviations in these means evaluated. Then new values of the K_La were computed based on assumed values of C^* and C_0 that deviated by one standard deviation from these means. These calculations suggest a possible error of up to 8% in the measured value of K_La.

Mass-transfer experiments were done in both the conventional tank configuration and the *ASSET* system at gas feed rates of 10, 20, and 30 L/min, corresponding to superficial gas velocities of 0.57 to 0.171 cm/s. As stated earlier, the conventional configuration was tested with an A310, A410, and R100 impeller, while the *ASSET* system was tested with the A310 and the A410 impeller. The performance of the conventional configuration serves as the base line against which the *ASSET* system is evaluated. A representative sample of the mass-transfer results obtained with the conventional configuration is presented in Figure 6. These data, which are for a gas feed rate of 0.171 cm/s, are typical of those obtained for all the gas feed rates tested, and show how the K_La increases with power input. Notice in particular that the results for the A310 and A410 impellers are nearly indistinguishable from each other as long as the K_La values are plotted against the power input per unit liquid volume in the tank (P/V). On the other hand, the K_La values for the radial flow (R100) turbine are consistently higher than those for the axial-flow turbines over the entire range of our experiments. This distinctiveness of the R100 impeller was greatest at the highest gas feed rate and was nonexistent at the lowest feed rate (0.057 cm/s). Another thing that is evident from the figure is that the value of K_La increases more slowly with increases in P/V for the R100 impeller than for the axial-flow

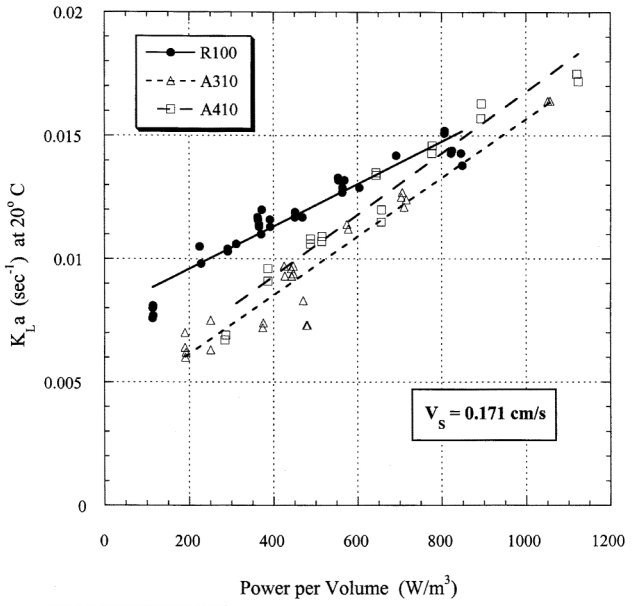

Figure 6. Effect of impeller type on the K_La obtained at a gas feed rate of 30 L/min in the conventional tank configuration.

Power input is presented per unit volume of liquid in the tank.

impellers. This result was observed at all gas flow rates tested with the conventional configuration.

Many investigators have observed and quantified the increase in K_La with increases in both power input and gas flow rate in mechanically agitated systems. Cooper et al. (1944) appear to have been the first to propose a correlation of these data of the form

$$K_La = k\left(\frac{P}{V}\right)^{\alpha}(V_S)^{\beta}, \tag{2}$$

where P is the power input, V is the liquid volume being stirred, and V_S is the superficial gas velocity. Since that time, many investigators have correlated their data with this equation and have obtained a wide range of values for the exponents α and β; namely, $0.32 \le \alpha \le 0.95$ and $0.2 \le \beta \le 0.7$ (such as Cooper et al., 1944; Fukuda et al., 1968; Linek et al., 1987; Liu et al., 1972; Richards, 1961; Van't Riet, 1979; Yagi and Yoshida, 1975). The values of these exponents appear to depend upon many factors, such as the size of the system, the impeller design, the ionic strength of the aqueous phase, and the method of measurement. Because of the discrepancy in the literature regarding the values of α and β, even for systems that superficially appear to be equivalent, it was imperative in the current investigation to make side-by-side measurements of the K_La in both the conventional configuration and the *ASSET* system.

We found that all of the mass-transfer data obtained with a particular impeller type in the conventional tank configuration could be correlated with Eq. 2, as shown in Figure 7 and 8. In particular, all the data obtained with the axial-flow impellers (the A310 an A410) were correlated by the following

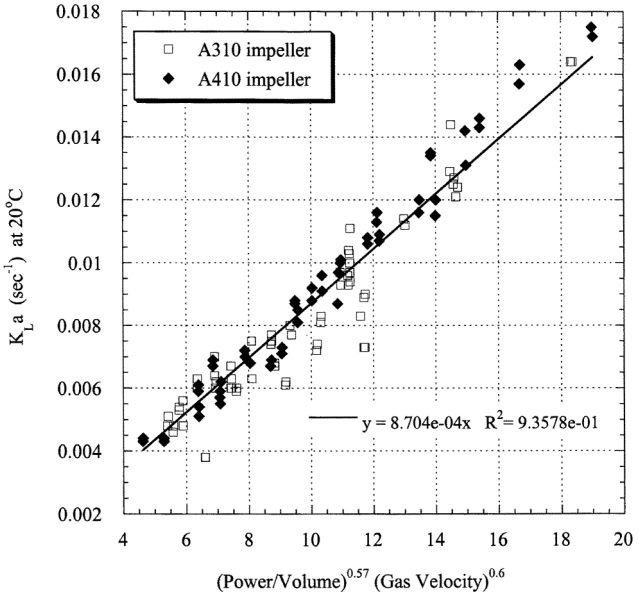

Figure 7. Power-law correlation of all the $K_L a$ data obtained with the conventional tank configuration equipped with an axial flow impeller.

All the A310 and A410 data are included.

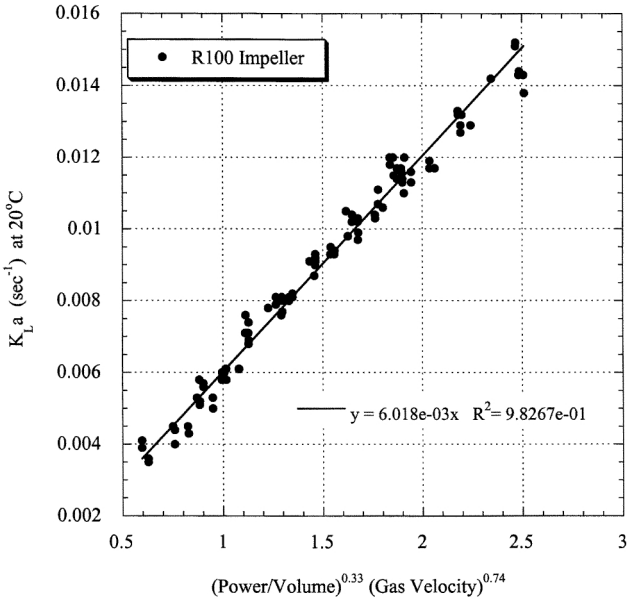

Figure 8. Power-law correlation of all the $K_L a$ data obtained with the conventional tank configuration equipped with the radial flow, R100 impeller.

equation:

$$K_L a = 8.704 \times 10^{-4} \left(\frac{P}{V}\right)^{0.57} (V_S)^{0.6}, \tag{3}$$

while for the radial-flow, R100 impeller

$$K_L a = 6.018 \times 10^{-3} \left(\frac{P}{V}\right)^{0.33} (V_S)^{0.74}, \tag{4}$$

where the units of $K_L a$, P/V, and V_S are s^{-1}, W/m^3, and cm/s, respectively. Notice that the exponents α and β are substantially different for the two impeller types, making it difficult to compare their relative performance on the same graph except in a format similar to Figure 6. It is also clear from Eqs. 3 and 4 that the dependence of $K_L a$ on power input is much weaker for the R100 impeller than for the axial-flow impellers, a result first deduced from Figure 6.

The use of Eq. 2 to correlate the mass-transfer data is appealing because it accounts for the influence of both power input and gas flow rate on the magnitude of $K_L a$. However, because our experiments do not span a wide range of conditions for either P/V or V_S, there is a significant degree of uncertainty regarding the values of the exponents α and β and even the appropriateness of Eq. 2 for correlating the data. As a counterpoint, a linear regression was done on each data set presented in Figure 6, and the straight lines obtained are presented in this figure. Visual inspection suggests a very good fit of the data. Indeed, the correlation coefficient (R value) for each linear fit was 0.958 or greater in all cases, supporting this conclusion. In general, for all of the experiments done with either the *ASSET* system or the conventional configuration, the value of the correlation coefficient obtained for the "power law" fit of each data set was virtually the same as that obtained for the corresponding linear fit. A linear fit suggests an exponent of 1.0, if one allows for the possibility of a y-intercept. Furthermore, our experimental data should not be expected to extrapolate to the origin, a feature inherent in the power-law correlation, the reason being that any further reduction of P/V in each data set would lead to an inoperative flooding condition. In conclusion, the point is not that the exponent on P/V should be unity, but rather the limited range of experimental conditions in our study do not allow us to obtain a reasonable value for either exponent, α and β.

The issue of primary interest in this investigation is the performance of the *ASSET* system relative to that of the conventional configuration under comparable conditions of power input and gas feed rate. To assure that the gas feed rate was indeed that fed into the tank through the sparge ring, so that a valid comparison could be made between the two configurations, the *ASSET* system was run with a shaft seal to eliminate the possibility of air induction down the central pipe. This comparison is provided in Figures 9, 10, and 11 for gas feed rates of 10, 20, and 30 L/min, respectively. In these figures, the performance of the *ASSET* system is compared with that obtained in the conventional configuration with the R100 impeller because, from the perspective of mass-transfer rate, the R100 impeller is the best performer among the various impeller alternatives in the conventional setup. The most important conclusion that can be drawn from these figures is that the *ASSET* system significantly outperforms the conventional setup over virtually the entire range of power inputs and gas flow rates studied. In particular, the $K_L a$ values obtained with the *ASSET* system are typically 30–50% larger than those obtained at equivalent operating conditions with the conventional configuration.

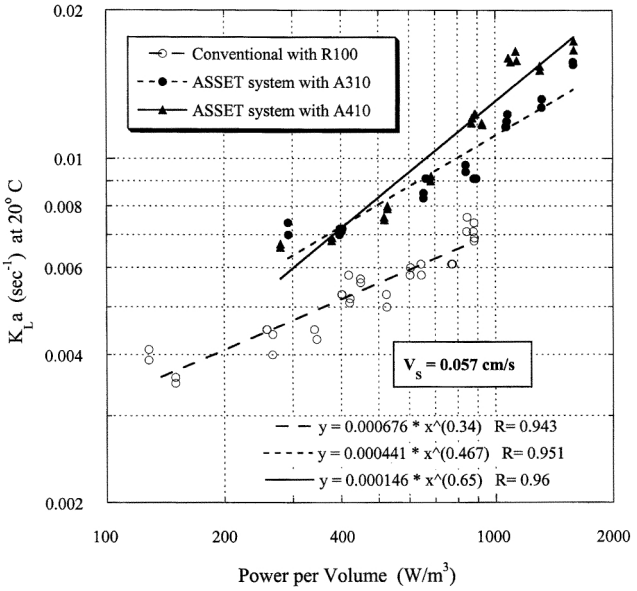

Figure 9. Values of $K_L a$ as a function of power input for the *ASSET* system with the A310 and A410 impellers at a gas feed rate of 10 L/min, with results for the R100 impeller in the conventional configuration at equivalent conditions.

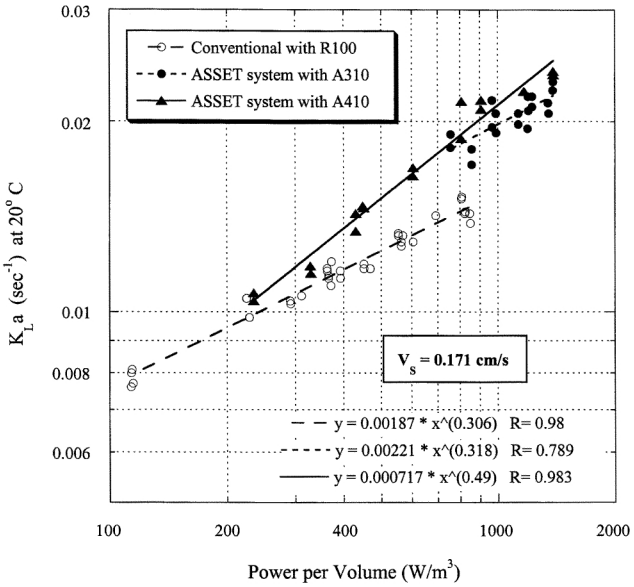

Figure 11. Values of $K_L a$ as a function of power input for the *ASSET* system with the A310 and A410 impellers at a gas feed rate of 30 L/min, with results for the R100 impeller in the conventional configuration at equivalent conditions.

The data in Figures 9–11 are plotted on a log-log scale to expose the power-law dependence of $K_L a$ on power input. The least-squares regression of each data set to a power-law model is also reproduced on the figures. The magnitude of the $K_L a$ values obtained with the A310 and A410 impellers in the *ASSET* system are quite similar. However, the data plots and the associated correlations indicate that the functional relationship between $K_L a$ and power input is distinctively different for the two impellers. This result is unexpected given their similar geometry and their nearly identical performance characteristics in the conventional tank configuration (see Figures 6 and 7). Another interesting result is that the exponent on P/V for the A310 and A410 impellers in the *ASSET* system is significantly different at a superficial gas feed velocity of 0.057 cm/s than at 0.114 and 0.171 cm/s. Consequently, it is not possible to obtain an estimate of the power-law dependence of $K_L a$ on the gas feed rate. (Such an estimate would have been questionable in any case, since experiments were done at only three different gas rates that span a limited range of values.) Notice in these figures that data for the R100 impeller were obtained only up to a power input of $\sim$ 900 W/m^3. Although we wanted to operate this conventional configuration at higher power inputs, our range of operating conditions was limited by the dynamometer spring balance, which has a force measurement limit of 10 lb$_f$. Because the R100 impeller has such a large Power number (see Figure 4), this spring force is reached at an impeller speed of $\sim$ 410 rpm, leading to a power input of 900 W/m^3.

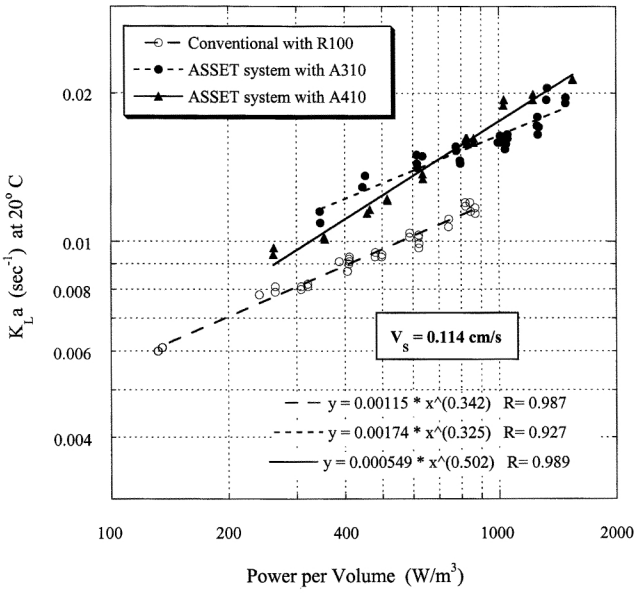

Figure 10. Values of $K_L a$ as a function of power input for the *ASSET* system with the A310 and A410 impeller at a gas feed rate of 20 L/min, with results for the R100 impeller in the conventional configuration at equivalent conditions.

As stated earlier, a potentially beneficial feature of the *ASSET* system is the ease with which it permits the impeller to draw in air through the central pipe to supplement the air being supplied through the sparge ring. The impact of this air induction phenomenon on the rate of gas–liquid mass transfer is illustrated in Figure 12. In this figure, the $K_L a$ values obtained in experiments done *without* a shaft seal and no gas feed rate are compared with the results obtained *with* a shaft seal (no air induction) and gas feed rates of 10, 20 and 30 L/min. In this figure, the dashed lines are the least-squares

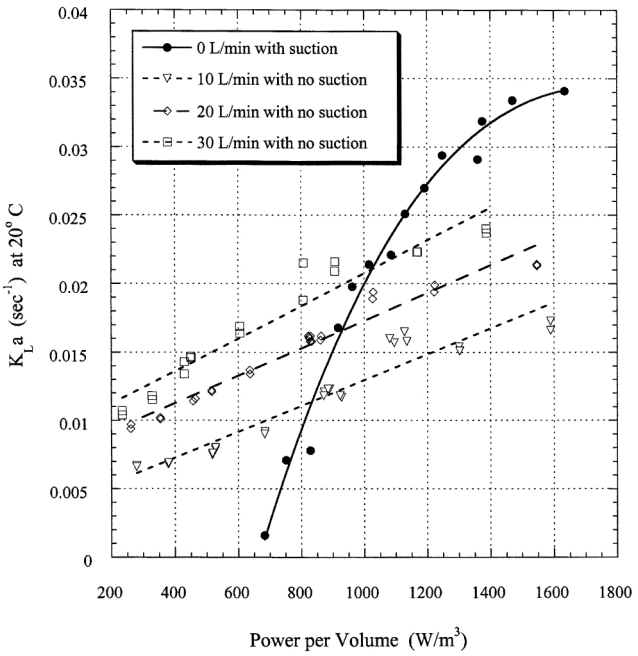

Figure 12. Effect on the volumetric mass-transfer coefficient of air induction due to suction down the central pipe in the *ASSET* system.

The solid curve is for the *ASSET* system operated without a shaft seal, with no air fed to the tank. The other three sets of data are for experiments done with the shaft seal in place, with air feed rates of 10, 20, and 30 L/min.

fits of the data sets with no air induction, while the solid line is a third-order polynomial fit of the data for the case in which the sole source of gas into the tank is via suction through the central pipe. It is evident from our experimental observations that gas begins to be drawn into the tank when the power input exceeds 650 W/m^3. At power inputs greater than this threshold value, it is evident from Figure 12 that air induction has a dramatic effect on the rate of mass transfer. In fact, at power inputs greater than ~ 1,000 W/m^3, the rate of mass transfer provided by suction alone exceeds that obtained with a shaft seal and gas sparging at 30 L/min.

Suspension of solids

The effectiveness of the *ASSET* system to promote the suspension of solids was determined in the following manner. The mixing tank was filled (to a height of 60.3 cm) with a 15 wt % solids suspension of 0.10-cm glass beads in water, and the height of the well-mixed region in the tank was measured as a function of the power input to the tank. The well-mixed region was evaluated visually as the zone in which the particles appeared uniformly dispersed; that is, the region in which the color and texture of the suspension appeared to be uniform. As long as this zone did not extend to the top surface of the water in the tank, there was a distinct boundary between the well-mixed zone and the region above it, where the concentration of glass beads was both smaller and position-dependent. The *ASSET* system was tested with both the A310 and the A410 impellers, and the two performed equivalently. The lack of distinction between the two impellers is not surprising since both have been optimized by Lightnin to produce the same, highly axial pumping profile; their primary distinction being the amount of gas that each can handle. (In these solids suspension experiments, the *ASSET* system was fitted with a shaft seal and no gas was fed to the system.)

The performance comparison between the *ASSET* system and the conventional tank configuration is presented in Figure 13. Notice that at a given power input the height of the well-mixed region is significantly larger in the *ASSET* system. Indeed, the power requirement to achieve a well-mixed region over 2/3 of the total liquid height (~ 40 cm) is approximately 50% less with the *ASSET* system than with the conventional configuration. Visual observations also revealed high axial velocities immediately adjacent to the vertical tank walls near the tank bottom, all around the circumference of the tank, in the *ASSET* system. Such flow intensities near the wall were not observed in the conventional tank except in the immediate vicinity of the four wall baffles. In the conventional configuration, the gathering of material in the corners of the tank was also apparent. No such dead spaces for materials accumulation exist in the *ASSET* system owing to the presence of the contoured bottom. The contours also allow the flow to "scrub" the bottom of the tank, as is apparent from the action of small tracer beads during independent, flow visualization experiments in plain water.

Conclusions

An alternative mixing-tank configuration is described that utilizes a set of six stationary fins enclosed in a shroud, as a substitute for traditional wall baffles, to remove the angular component of velocity (swirl) imparted to the liquid in a mix-

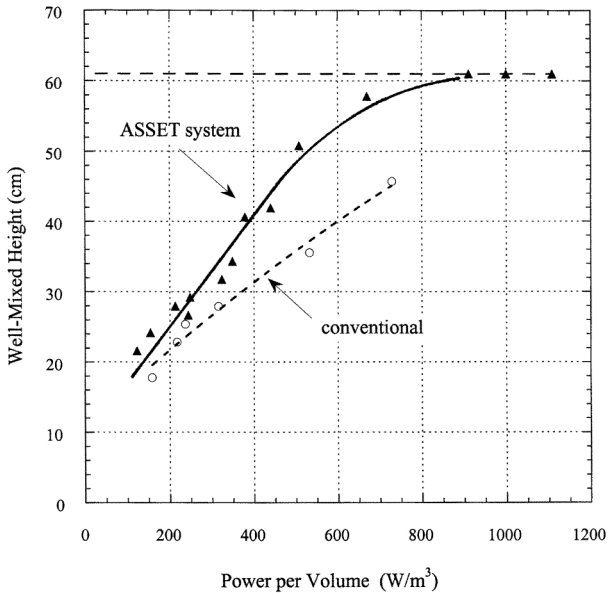

Figure 13. The relative ability of the *ASSET* system to suspend solid particles.

The data show the perceived height of the well-mixed solids suspension in the tank as a function of power input for both the *ASSET* system and the conventional configuration. Data are for both the A310 and A410 impellers. The suspension is 15 wt. % of 0.1-cm-diam glass beads in water.

ing tank by the clockwise rotation of the impeller. This shroud assembly, when placed in close proximity to the impeller, reduces rotational flows to a minimum. In addition, a toroidally shaped tank bottom is described that eliminates the stagnation zones present in conventional, flat-bottomed tanks with wall baffles, and capitalizes on the strongly directional pumping profile of axial-flow impellers to provide a highly efficient recirculatory flow pattern, particularly with regard to the off-bottom suspension of solid particles. When the shroud assembly is combined with this toroidally shaped bottom, a new mixing-tank configuration with several beneficial qualities is created. This new configuration, termed the *ASSET* system, has a low power consumption profile, with a Power number at high Reynolds number that is ~ 50% greater than that for axial flow impellers and a factor of 10 lower than that for radial flow impellers in traditional tank configurations. Yet in applications involving gas–liquid dispersions, the *ASSET* system produces volumetric mass-transer coefficients that are typically 30–50% higher than those obtained with a *radial* flow impeller in a conventional mixing-tank setup. This level of improvement strongly suggests that the *ASSET* system is making more efficient use of the power input to the mixing process. This increased effectiveness should yield improvements in mixing applications beyond the scope of gas–liquid dispersions.

One interesting feature of the new mixing system is the ease with which it draws air down into the impeller region to provide high rates of gas–liquid mass transfer without any additional gas sparging. This performance feature may prove useful in industrial applications that require the contacting of liquids or slurries with toxic, reactive, and/or corrosive gases. In such circumstances, the cost and concern over the use of a compressor to deliver the gas could be eliminated in favor of an *ASSET* system that could continuously recycle gas out of the vapor space in the tank and down the central pipe into the liquid phase. Thus, the toxic gas could be fed to the vapor space only in quantities that offset the amount being transferred to (and reacted with) the liquid.

One disadvantage of the *ASSET* system as currently configured is its greater tendency to flood with gas, relative to axial-flow impellers in conventional tanks. The reason appears to be due to the presence of the stationary fins and cylindrical shell, all of which tend to restrict gas movement away from the impeller blades except in the downward direction of the flow exiting from the impeller. This greater tendency of the current *ASSET* system configurations to flood at high gas feed rates and low power inputs will be examined in greater detail in future experiments. Other disadvantages from a commercial viewpoint include the added capital cost of the special tank needed and the possible difficulties associated with cleaning the shroud assembly between semibatch operations. On the other hand, the absence of baffles should simplify the cleaning of the tank walls.

At this stage, no attempt has been made to optimize the design beyond the efforts made to shape the fins to eliminate swirl. One might anticipate, for example, that additional performance gains can be achieved by altering the size and position of the shroud assembly, or by optimizing the shape of the antiswirl fins for specific impellers to produce the best possible flow at the lowest expenditure of energy. Optimization of the fins could also reduce the tendency of the *ASSET* system to flood. In conclusion, we believe that the new mixing configuration presented in this article holds great promise for minimizing energy consumption while increasing mixing performance in a wide range of industrial applications.

Acknowledgment

The authors thank *Lightnin*, a division of General Signal, Inc., for their financial support, which made this investigation possible. The authors greatly appreciate the advice and technical support provided by Tom Post, Richard Howk, and James Stanton of *Lightnin*. We are also indebted to Mike Stone of the UR Chemical Engineering Department for his many hours of help and guidance on the mechanical aspects of experimental setup, and to Thor Olsen for help with the computer interface. In addition, we thank Bichnya Nguyen and Archie Kaul, former Chemical Engineering undergraduates, for their contributions to the project.

Literature Cited

Aeschbach, S., and J. R. Bourne, *Chem. Eng. J.*, **4**, 234 (1972).
Bakker, A., and H. E. A. VandenAkker, *Inst. Chem. Eng. Symp. Ser.*, **121**, 153 (1990).
Carpenter, C. M., "Mixing in an Unconventional Tank Configuration: Power Consumption, Gas-Liquid Mass Transfer, and Solids Suspension Studies," M.S. Thesis, Univ. of Rochester, Rochester, NY (1998).
Cooper, C. M., G. A. Fernstrom, and S. A. Miller, *Ind. Eng. Chem.*, **36**, 504 (1944).
Eckenfelder, W. W., Jr., *Industrial Water Pollution Control*, McGraw-Hill, New York, p. 66 (1966).
Fukuda, H., Y. Sumino, and T. Kansaki, *J. Ferment. Tech.*, (Jpn), **46**, 829 (1968).
Görtler, H., *ZAMM*, **21**, 250 (1941).
Hyman, D., *Adv. Chem. Eng.*, **3**, 119 (1962).
Jahoda, M., and V. Machon, *Chem. Eng. Technol.*, **17**, 95 (1994).
Jameson, G. J., *Chem. Process Eng.*, **43**(9), 478 (1962).
Lee, J. H., and N. R. Foster, *Appl. Catal.*, **63**, 1 (1990).
Lessen, M., "Down-Flow Batch Mixing System," U.S. Patent No. 5,454,986 (1995).
Linek, V., V. Vacek, and P. Benes, *Chem. Eng. J.*, **34**, 11 (1987).
Liu, M. S., R. M. R. Branion, and D. W. Duncan, *J. Water Pollut. Cont. Fed.*, **44**, 34 (1972).
Mann, R., *Inst. Chem. Eng. Symp. Ser.*, **94**, 335 (1985).
Nagata, S., *Mixing: Principles and Applications*, Halsted Press, New York (1975).
Oldshue, J. Y., *Fluid Mixing Technology*, McGraw-Hill, New York (1983).
Oldshue, J. Y., *Ind. Eng. Chem.*, **57**(11), 115 (1965).
Oldshue, J. Y., and N. R. Herbst, *A Guide to Fluid Mixing*, Mixing Equipment Co., Rochester, NY (1990).
Oldshue, J. Y., T. A. Post, R. J. Weetman, and K. Coyle, *Proc. Eur. Conf. Mixing*, **6**, 345 (1988).
Richards, J. W., *Prog. Ind. Microbiol.*, **3**, 143 (1961).
Rushton, J. H., E. W. Costich, and H. J. Everett, *Chem. Eng. Prog.*, **46**, 395 (1950).
Rushton, J. H., E. W. Costich, and H. J. Everett, *Chem. Eng. Prog.*, **46**, 465 (1950).
Schlichting, H., *Boundary Layer Theory*, Chap.17, McGraw-Hill, New York (1968).
Van't Reit, K., *Ind. Eng. Chem. Proc. Des. Dev.*, **18**, 357 (1979).
Yagi, H., and F. Yoshida, *Ind. Eng. Chem. Proc. Des. Dev.*, **14**, 488 (1975).
Yoshida, M., A. Kitamura, K. Yamagiwa, and A. Ohkawa, *Can. J. Chem. Eng.*, **74**, 31 (1996).
Zhou, G., and S. M. Kresta, *AIChE J.*, **42**, 2476 (1996).

Manuscript received June 29, 1998, and revision received June 25, 1999.